Ecological Indicators 102 (2019) 734–745

Contents lists available at ScienceDirect

Ecological Indicators

journal homepage: www.elsevier.com/locate/ecolind

Original Articles

Using multi-indices approach to quantify mangrove changes over the Western Arabian Gulf along Saudi Arabia coast

Wenzhao Li[a], Hesham El-Askary[b,c,d,*], Mohamed A. Qurban[e,f], Jingjing Li[g], K.P. ManiKandan[e], Thomas Piechota[c]

[a] Computational and Data Sciences Graduate Program, Schmid College of Science and Technology, Chapman University, Orange, CA 92866, USA
[b] Center of Excellence in Earth Systems Modeling & Observations, Chapman University, Orange 92866, CA, USA
[c] Schmid College of Science and Technology, Chapman University, Orange 92866, CA, USA
[d] Department of Environmental Sciences, Faculty of Science, Alexandria University, Moharem Bek, Alexandria 21522, Egypt
[e] Center for Environment and Water, The Research Institute, King Fahd University of Petroleum and Minerals (KFUPM), Dhahran 31261, Saudi Arabia
[f] Geosciences Department, The College of Petroleum Engineering & Geosciences, King Fahd University of Petroleum and Minerals (KFUPM), Dhahran 31261, Saudi Arabia
[g] Department of Geosciences and Environment, California State University Los Angeles, CA 90032, USA

ARTICLE INFO

Keywords:
Mangrove
Arabian Gulf
Google Earth Engine
Landsat
Ecological indices
Change detection
Classification methodologies

ABSTRACT

Mangroves habitat present an important resource for large coastal communities benefiting from activities such as fisheries, forest products and clean water as well as protection against coastal erosion and climate related extreme events. Yet they are increasingly threatened by natural pressure and anthropogenic activities. We observed an inaccurate distribution of mangroves over the Western Arabian Gulf (WAG) which is a vital habitat and resource for the local ecosystem, according to the United Stated Geological Survey (USGS) mangrove database through spectral analysis. Change detection analysis is conducted on mangrove forests along the Saudi Arabian coast of the WAG for the years 2000, 2010 and 2018 using Landsat 7 & 8 data. Three supervised classification methodologies are employed for mangrove mapping, including Supported Vector Machine (SVM), Decision Tree (DT), referred to as Classification and Regression Trees (CART) and Random Forest (RF). CART's accuracy was recorded to be > 95% while other classifiers were > 90%. The CART supervised learning classifier, mapping mangroves' distribution and biomass using Google Earth Engine (GEE) online platform, indicates an overall increase in the northern Tarut Bay and Tarut Island, by 0.21 km^2 from 2000 to 2010 and by 1.4 km^2 from 2010 to 2018. The increase might be due to mitigation strategies such as mangrove breeding and plantation. It can be challenging to detect changes in certain regions due to the inadequate resolution of Landsat where submerged mangroves can be confused with salt marshes and macro algae. We employed a new method to identify and analyze submerged mangrove forests distribution via a submerged mangrove recognition index (SMRI) and Normalized Difference Vegetation Index (NDVI) in Abu Ali Island. Our results show the robustness of SMRI as an effective indicator to detect submerged mangroves in both high and medium spatial resolution satellite images. NDVI values differentiated submerged mangroves from tidal flats between Landsat 7 & 8 as well as during conditions of low and high tides. High resolution WorldView-2 image showed agreement of mangroves distribution with the SMRI and NDVI results.

1. Introduction

Mangrove forests are present in the intertidal zone, located within small groups of trees and shrubs in the harsh interface between sea and land. They are distributed largely in the tropical and subtropical areas between 30°N and 30°S latitude. As a habitat to rich and biologically complex species, they are one of the most productive ecosystems in the world (Donato et al., 2011), providing considerable services to human communities with ecological and economic values to protect shoreline from storms, erosion, and sedimentation (Moore et al., 2015), as well as providing nutrients for algae blooms (Li et al., 2017; Li et al., 2018). The protective role of mangrove forests was also recognized during

Abbreviations: SMRI, submerged mangrove recognition index; NDVI, Normalized Difference Vegetation Index; GEE, Google Earth Engine; WAG, Western Arabian Gulf

* Corresponding author at: Schmid College of Science and Technology, Chapman University, 1 University Drive, Orange, CA 92866, USA.
E-mail address: elaskary@chapman.edu (H. El-Askary).

https://doi.org/10.1016/j.ecolind.2019.03.047
Received 10 October 2018; Received in revised form 21 March 2019; Accepted 24 March 2019
1470-160X/

Asian Tsunami of 2004 and other natural disasters such as hurricanes (Danielsen, 2005; Kathiresan and Rajendran, 2005). The analysis of the economic values of the mangrove forests is necessary for integrated land use planning and environmental decision-making (Vo et al., 2012). A Mangrove Quality Index (MQI), ranking 1 (worst) to 5 (excellent), was developed to evaluate the overall mangrove health status of mangrove ecosystems in Matang, Malaysia (Faridah-Hanum et al., 2019).

In addition, mangrove forests, acting as significant carbon sinks, play an important role in climate change (Donato et al., 2011). However, mangroves are threatened due to both anthropogenic and natural stressors. For instance, over the western Arabian Gulf, increased soil contaminations of heavy metals was found in the mangrove habitats (Al-Kahtany et al., 2018; Almahasheer, 2019). One third of their forests has been lost in the past half century (Alongi, 2002). It is estimated that 35% of the mangrove forests were lost during 1980 to 2005 (Millennium Ecosystem Assessment, 2005) in a much faster declining rate than coral reefs and inland tropical forests (Duke et al., 2007). Mangrove habitat land use change is used as an indicator for environmental quality, for instance, such a change can affect soil microbial biomass (Dinesh and Ghoshal Chaudhuri, 2013), as well as intertidal fish communities (Ellis and Bell, 2013). If no actions are taken to protect the mangrove ecosystem, 30–40% of coastal wetlands and 100% of mangrove forest could lose their functionalities in the next 100 years with the present declining rate (Shapiro et al., 2015).

Mangrove forests cover around 152,000 km^2 in 123 countries and territories in the tropics and subtropics of the world (Spalding et al., 2010), among which Middle East region has 624 km^2, about 0.4% of global coverage. Arabian Gulf, one of the most important inland sea at this region, is little known about its coverage and distribution of mangrove forests. The Arabian Gulf is a shallow basin of an average depth of 35 m, extending approximately 24°–30°N and 48°–56°E (Al-Muzaini and Jacob, 1996). Its coastlines, which is the most arid in the world, were formed in the past 3000–6000 years (Burt, 2014). The water temperature vary from around 12 °C to 35 °C (Price et al., 1993), and the surface temperature in intertidal zones can exceed 50 °C in the summer (Burt, 2014). The salinity in the Arabian Gulf is as high as 43 psu and may even reach 70–80 psu in tidal pools and lagoons. This is due to the high-latitude geographical location, high evaporation rates, as well as relative shallowness. In such an extreme environment, most of the marine species in the Arabian Gulf reach their tolerance limits (Price et al., 1993). Mangroves, however, are able to survive in this region because they tolerate the high salinity at early stages of development (Naser and Hoad, 2011). One type of mangroves, *Avicennia marina*, can be sparsely found at the southern shores, confined to sheltered coastal areas along the coastlines of Saudi Arabia, Arab Emirates and Qatar (Burt, 2014). Despite the low volume, low diversity and intermittent occurrence of mangroves, the presence is of significant ecological importance in this region. Mangroves are among the only trees in the desert landscape, offering food for livestock and other wild animals. They support a variety of essential species of birds, fish, shrimps and turtles, contributing substantially to the coastal productivity (Al-Maslamani et al., 2013). It has been reported that Tarut Bay alone has lost a significant 55% mangrove forests (mostly in the south part) from 1972 till 2011 (Almahasheer et al., 2013). This is attributed to human and environmental pressures such as pollutants, land reclamation and urban encroachment. On the other hand a regional research of decadal changes of the Red Sea mangrove forest showed a slight increase of its coverage (Almahasheer et al., 2016). Fortunately, the mangrove forests has been in a recovery process with small increase by plantation activities by both government (i.e., the Ministry of Agriculture) and industry (Saudi-Aramco 2016) in Saudi Arabia. As early as 1970s, vegetation indices had been used for quantitative measurement of vegetation conditions (Rouse et al., 1973; Gitelson et al., 1996; Ahamed et al., 2011). High spatial resolution remote sensing imagery could generate various vegetation indices, such as Normalized Difference Vegetation Index (NDVI, NDVI2), Normalized Difference Red Edge index (NDRE, NDRE2), Green Normalized Difference Vegetation Index (GNDVI) and Chlorophyll Vegetation Index (CVI), which have been widely investigated to mangrove and other species, such as mangrove canopy chlorophyll concentration (Heenkenda et al., 2014, Heenkenda et al., 2015, Vincini et al., 2007, 2008), feedstock biomass production (Ahamed et al., 2011), and low and high density mangrove estimation (Mutanga et al., 2012; Al-Ali et al., 2015; Almahasheer et al., 2013, Almahasheer et al., 2016).

Mangroves have very distinct spectral features in remote sensing data, especially in the spectral ranges corresponding to the visible red, near-infrared, and mid-infrared, making it easier to classify than other land cover types. The best combination of spectral bands to detect mangroves are Landsat 7 bands 3 (0.63–0.69 μm), 4 (0.77–0.90 μm), 5 (1.55–1.75 μm), and 7 (2.09–2.35 μm) (Giri, 2016). Therefore, indices like the Normalized Difference Vegetation Index (NDVI) are useful in identification it has been employed for other applications (Kim et al., 2014; Whitney et al., 2018). Recent advancement in computing and information technology, image-processing methodologies, as well as the availability of remote sensing data, have provided an opportunity to monitor mangroves at regional and global scales on a consistent and regular basis. Meanwhile, there has been an increase in high-performance cloud computing platforms, such as the NASA Earth Exchange (NEX), Amazon Web Service (AWS), and Google Earth Engine (GEE). The advantages of cloud computing include the parallel computing, offering nearly unlimited computer processing capabilities, as well as free access to a large volume of satellite remote sensing data stored in the remote cloud drives. This eliminates the need for large external hard disk storage and facilitates easy data access. For example, GEE provides preprocessed Sentinel data (2014–present), Landsat data (1982-present), as well as advanced classification machine learning algorithms accessible through JavaScript and Python programs (Giri et al., 2015). One research project utilized GEE to analyze the changes of mangrove forests over 30 years in Thailand (Pimple et al., 2018). It is noteworthy that this Thailand mangrove study didn't use the Landsat 7 data after 2003 and had a missing scene in the year of 2012. This is because Landsat 7 Enhanced Thematic Mapper (ETM) sensor had a failure of the Scan Line Corrector (SLC) on 31 May 2003. Since that time all Landsat ETM data has wedge-shaped gaps on both sides of each scene, resulting in approximately 22% of data loss.

Mangrove forests mapping methods are usually based on a single-day imagery analysis, which can suffer from low or high tides. Such analysis can suffer by not taking the tide levels into consideration given that mangrove forests are periodically submerged by tides. This can impose a problem of over or under estimation in mangrove mapping when the images are observed during high-tide periods. Since mangroves grow along often-narrow extent along coastlines, detailed mangrove ecosystem characterization becomes difficult with moderate-resolution (30 m) satellite data and there is a need for high-resolution imagery to gain more accurate mapping results at different tide levels (Green et al., 1998). A recent study proposed a new method to identify submerged mangrove forests via a submerged mangrove recognition index (SMRI) using high-resolution satellites' images, which considered different spectral signatures of mangroves under both low and high tide levels (Xia et al., 2018). However, due to naturally and/or human factors, mangrove communities along the Arabian Gulf coastlines covering more than 165 km^2 are predominantly separated from each other (Almahasheer, 2018). This fragmentation brings massive cost to study mangrove at a regional scale with only using high resolution remote sensing images. For example, SA has a 700 km long coastline in WAG (Bird, 2010). This will cost around $26,600 for getting entire coastline using WorldView-2 images with 8-bands for one time period (calculated from price listed in www.landinfo.com: $19/$km^2$ with 2 km minimum order width). The mangrove change detection study of two periods will cost double the price. Therefore, there is a need to improve mangrove detection methods through free accessible medium-resolution satellite imagery (such as Landsat 7/8). Here we employed high resolution

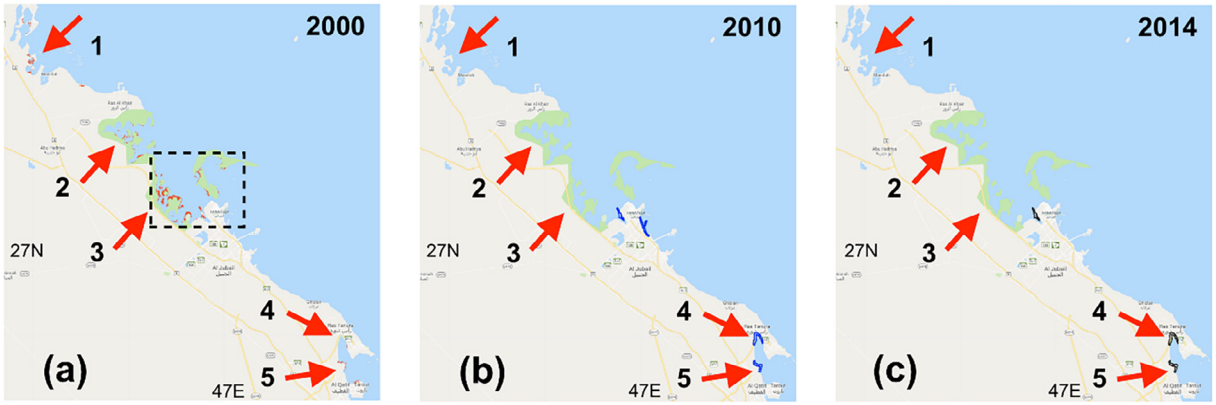

Fig. 1. Mangrove distribution in WAG for regions 1: Manifah, 2: Al-Khair, 3: Jubail, 4: North Tarut Bay, 5: North Middle Tarut Bay using (a) USGS Global Mangrove Forest Distribution of year 2000 (red color) (b) World Atlas of Mangroves of the year 2010 (blue color) (c) Mangrove Forest Biomass of the year 2014 (black color). The red arrows point to the mangroves, and black box highlights the massive mangrove coverage of USGS data.

images for selected regions for validation purposes.

We present a multi-indices based approach, using NDVI and SMRI, for long term mapping of mangrove forests in the WAG region along the Saudi Arabia coast. In this study, we evaluate the accuracy of three existing mangrove forests datasets and for the first time, incorporated SMRI as a new assessment for detecting submerged mangrove at different tide levels over the WAG region using Landsat medium-resolution remote sensing images.

2. Materials and methods

2.1. Data

Three mangrove datasets were used in this research: 1) USGS Global Mangrove Forest Distribution of year 2000 (Giri et al., 2011). This dataset was generated using Landsat satellite images of more than 1000 scenes obtained from the USGS Earth Resources Observation and Science Center (EROS). Mangroves were classified using hybrid supervised and unsupervised digital image classification techniques. 2) World Atlas of Mangroves. This dataset shows the global distribution of mangroves, and was produced as a joint initiative of the Food and Agriculture Organization of the United Nations (FAO), the International Tropical Timber Organization (ITTO), International Society for Mangrove Ecosystems (ISME), UN Environment World Conservation Monitoring Centre (UNEP-WCMC) (Spalding et al., 2010), United Nations Educational, Scientific and Cultural Organization's Man and the Biosphere Programme (UNESCO-MAB), United Nations University Institute for Water, Environment and Health (UNU-INWEH), and The Nature Conservancy (TNC). 3) Global Distribution of Modelled Mangrove Biomass (2014) (Hutchison et al., 2014). This dataset was developed by the Department of Zoology in University of Cambridge, with the support from The Nature Conservancy. It shows the global patterns of aboveground biomass of mangrove forests based on a review of 95 field studies on carbon storage and fluxes in mangroves world-wide.

Two kinds of remote sensing images are used here: 1) WorldView-2 image. WorldView-2 is a high-resolution satellite launched on October 8, 2009 from Vandenberg Air Force Base, CA. WorldView-2 collects 46-centimeter (cm) panchromatic and 1.85-meter (m) multispectral imagery. In this research, we obtained the image of four traditional bands (i.e. blue, green, red and NIR) over the Abu Ali Island during September 2017 to study for the submerged mangrove detection. 2) Landsat 5, Landsat 7, and Landsat 8 Surface Reflectance Tier 1 dataset from the Landsat 5 TM, Landsat 7 ETM + sensor and Landsat 8 OLI/TIRS sensors. These images contain 4 visible and near-infrared (VNIR) bands of 30 m resolution for Landsat 7 (5 VNIR bands for Landsat 8), 2 shortwave infrared (SWIR) bands of 30 m resolution processed to orthorectified surface reflectance, and one thermal infrared (TIR) band of resampled 30 m resolution for Landsat 5/7 (2 thermal bands for Landsat 8) processed to orthorectified brightness temperature. The surface reflectance dataset was provided from GEE. They have been atmospherically corrected using The Landsat Ecosystem Disturbance Adaptive Processing System (LEDAPS), and include a per-pixel saturation mask and a cloud, shadow, water and snow mask produced using C Function of Mask (CFMASK). In this study, we utilized Landsat 5 image of 1985, Landsat 7 images of 2000, 2010 and 2018, and Landsat 8 images of 2018 for the aforementioned three mangrove datasets for inter comparison. Landsat 7 and 8 images were also used for detecting the mangrove changes between 2000, 2010, and 2018. Moreover, we obtained and processed Landsat 7 and Landsat 8 images of 2017 to quantify the submerged mangrove in Abu Ali Island based on tidal data. The tidal data was accessed from the harmonic model by WorldTides™ (https://www.worldtides.info) that uses a number of public and licensed sources for tidal predictions as well as land-based station observations from tide gauges and satellite observations when available for the maximum accuracy. Since tides are caused by the gravitational pull on water from the sun, moon, and other planets, hence the gravitational pulls' frequencies are well known, thus harmonic analysis models are employed here for future water levels prediction based on past observations.

2.2. Study region

Fig. 1 shows mangrove distribution for the years 2000, 2010 and 2014, respectively, using the three existing mangrove datasets over the WAG. The 2000 image from USGS Global Mangrove Forest Distribution is accessed through GEE searching tool, and 2010 image from World Atlas of Mangroves and 2014 image from Mangrove Forest Biomass are converted into GeoTIFF format files, then imported into GEE. Along the coast of Saudi Arabia, five regions are studied based on the mangroves' distribution: 1. Manifah, 2. Al-Khair, 3. Jubail, 4. North Tarut Bay, and 5. North Middle Tarut Bay, all marked by correspondent numbers in the Fig. 1. Fig. 1 shows obvious differences among the three datasets, for instance, mangroves in region 1 (Manifah) and region 2 (Al-Khair) can be found in 2000 (pointed at by the red arrow), but disappeared in 2010 and 2014. Mangroves of region 3 (Jubail) are observed in all three years, with the highest coverage in 2000 highlighted in black squared area, whereas in 2010 and 2014 the mangrove only be marked in the Gurmah Island (at location 3 in green color 2010 and red color 2014).

On the north side of region 4 (North Tarut Bay), both the 2010 (Fig. 1b) and 2014 (Fig. 1c) are marked with a mangrove distribution (pointed by a red arrow) near Ras Tanura, but not much appearing in the 2000 data (Fig. 1a). In addition, mangroves are distributed in region

5 (North Middle Tarut Bay) in the 2010 data (pointed by a red arrow in Fig. 1b) and 2014 (Fig. 1c), while they do not appear that much in 2000 (Fig. 1a). Therefore, it is clear that large discrepancies were identified among these three years datasets. This could be explained either due to a massive decline and disappearance of mangroves in 2000 in regions 1 &2&3 after 2010 or a misclassification of the mangrove dataset by USGS accounting for other species as mangroves. Therefore, accurate assessment and validation work is highly needed to avoid misleading datasets, especially if it were to be used to build models for future mangrove change detection researches and for stakeholders and decision makers. In this study, we conducted a spectral analysis over the commonly recognized mangrove areas (in regions 3, 4 and 5), and from uncertain mangrove areas (region 3). The unique spectral signatures from mangrove habitats could help accurately decide on the consistency of distribution for mangrove habitats across the different data sets and at different locations.

2.3. Methodology

2.3.1. Classification methods

The workflow of generation and validation of mangrove classification model along with the procedures of classifying mangrove forests follow the workflow of the change detection analysis of coral reef habitat using Landsat data in the Red Sea (Hurghada, Egypt) (El-Askary et al., 2014). The Landsat 7&8 images of the year 2018 are used to generate different mangrove detection models, including Supported Vector Machine (SVM), Decision Tree (DT), referred to as Classification and Regression Trees (CART) and Random Forest (RF). The results of these models are evaluated by the accuracy (generated from confusion matrices), and by comparing with high-resolution image from Google Earth. Then the most effective models are selected to classify the mangrove distribution for the areas of interest among the year of 2000, 2010, and 2018 using Landsat 7&8 images. It is noteworthy that Landsat 5 did not provide image after August 1st 2002 in these regions. Alternatively, Landsat 7 images during the year 2010 were processed with GEE built-in mosaicking method to guarantee ideal results.

2.3.1.1. CART. CART, a supervised classification mining method, is used here to construct a decision binary tree structure through iterative analysis based on the training dataset that consists of features (i.e. spectral signatures) and target variables (i.e. mangrove or other classes) (Breiman, 1998). It has been widely used in land use analysis and change detection (Lawrence and Andrea, 2001), wetlands and mangrove distribution classification (Pantaleoni et al., 2009; Zhao et al., 2014). In this research, we used the maximum tree depth which controls the maximum number of allowed levels below the root node to construct the decision tree. Normally, the larger the maximum tree depth value, the more complex the decision tree and the higher the classification accuracy. Through multiple trials and the 10-fold cross validation, a maximum tree depth value of ten was selected for the CART classification.

2.3.1.2. SVM. The SVM machine learning algorithm, a well-adapted technique for solving non-linear, high dimensional space classifications, is used here as it showed a good performance in mangrove satellite sensing (Heenkenda et al., 2014; Heumann, 2011; Kanniah et al., 2015; Wang et al., 2018). It was found that SVM has better performance than maximum likelihood and artificial neural network classifiers using Landsat TM image (Pal and Mather, 2005). Moreover, SVM outperforms discriminate analysis and decision-tree algorithms for airborne sensor data (Foody and Mathur, 2006). SVM uniqueness from other traditional classification approaches stems from its ability to create a hyperplane through n-dimensional spectral-space. This plane separates classes (mangroves versus others) based on a user defined kernel function (linear in our case) and parameters that are optimized using machine-learning to maximize the margin from the closest point to the hyperplane.

2.3.1.3. RF. RF is a relatively new technique for mangrove species mapping, though it has been widely applied in landscape (Duro et al., 2012; Li et al., 2016) and plant species (Le Louarn et al., 2017; Ng et al., 2017) classification with different sensors in recent years. The RF algorithm is an ensemble algorithm for supervised classification based on CART. However, by combining the characteristics of CART together with further bootstrap aggregating, and random feature selecting, independent predictions can be established and therefore improve accuracies. For the RF algorithm, the tuning parameters mainly included “number of features”. This controls the size of a randomly selected subset of features at each split in the tree building process, which could have sensitive impact on classification (Duro et al., 2012). The other tuning parameter also includes the maximum number of trees (Su et al., 2017). In this research, the maximum level of trees used was five above which the accuracy did not change much.

2.3.2. Submerged mangrove recognition index (SMRI)

Most previous change detection research of mangrove forests are based on remote sensing images captured at different dates, not considering the impacts of tide level changes (Collins et al., 2017; Li et al., 2013; Rogers et al., 2017; Xia et al., 2018). However, mangrove forests are distributed near the land–sea interface, such as shorelines and in elongated or fragmented patches, especially in the WAG. These mangroves periodically receive inundation of sea water, where the fluctuating water underneath the canopy dramatically changes the spectral signatures as observed using satellite images. Therefore, it is difficult to retrieve accurate mangrove information using the methods based on single-day remote sensing imagery comparison of vegetation indices (i.e. NDVI). Recently, Xia et al. (2018) proposed a submerged mangrove recognition index (SMRI) by using high-resolution GF-1 images in both low and high tides, to describe the unique spectral signature of submerged mangroves and to distinguish mangroves forests submerged by different tide levels. The detailed form of the SMRI index is based on a combination of NDVI (Rouse et al., 1973) and near-infrared bands, shown below:

$$\mathrm{SMRI} = (NDVI_l - NDVI_h) \times \frac{NIR_l - NIR_h}{NIR_h} \tag{1}$$

$$NDVI_l = \frac{NIR_l - R_l}{NIR_l + R_l} \tag{2}$$

$$NDVI_h = \frac{NIR_h - R_h}{NIR_h + R_h} \tag{3}$$

where $NDVI_l$ and $NDVI_h$ are the NDVI values at low tide and high tide, respectively. NIR_l and NIR_h are the reflectance values of the near-infrared band at low and high tide, respectively. R_l and R_h are the reflectance values of the red band at low and high tide, respectively. In this research, we apply this index for detecting the submerged mangrove forests with Landsat medium-resolution imagery.

We also conducted studies to look at the effects of tide levels on the mangrove classification. WorldView-2 image was utilized to provide training data and validation for unsupervised classification cluster of mangrove in Abu Ali Island during the limited time period of September 2017. Landsat 7&8 images were used to implement the unsupervised classification method to explore the attributes of submerged mangroves for the same time period over the same region. All of the images were preprocessed, subset for coastal areas only and not including terrestrial vegetation and masked for marine habitats only and excluding water and land. We also applied the NDVI and SMRI, a new indicator to improve the submerged mangrove detection and to detect tidal impacts. It is noteworthy that all the Landsat and WorldView-2 images are visualized with false color configurations (R: near infrared band, G: red band, B: green band) to highlight the vegetation as red areas. Supervised

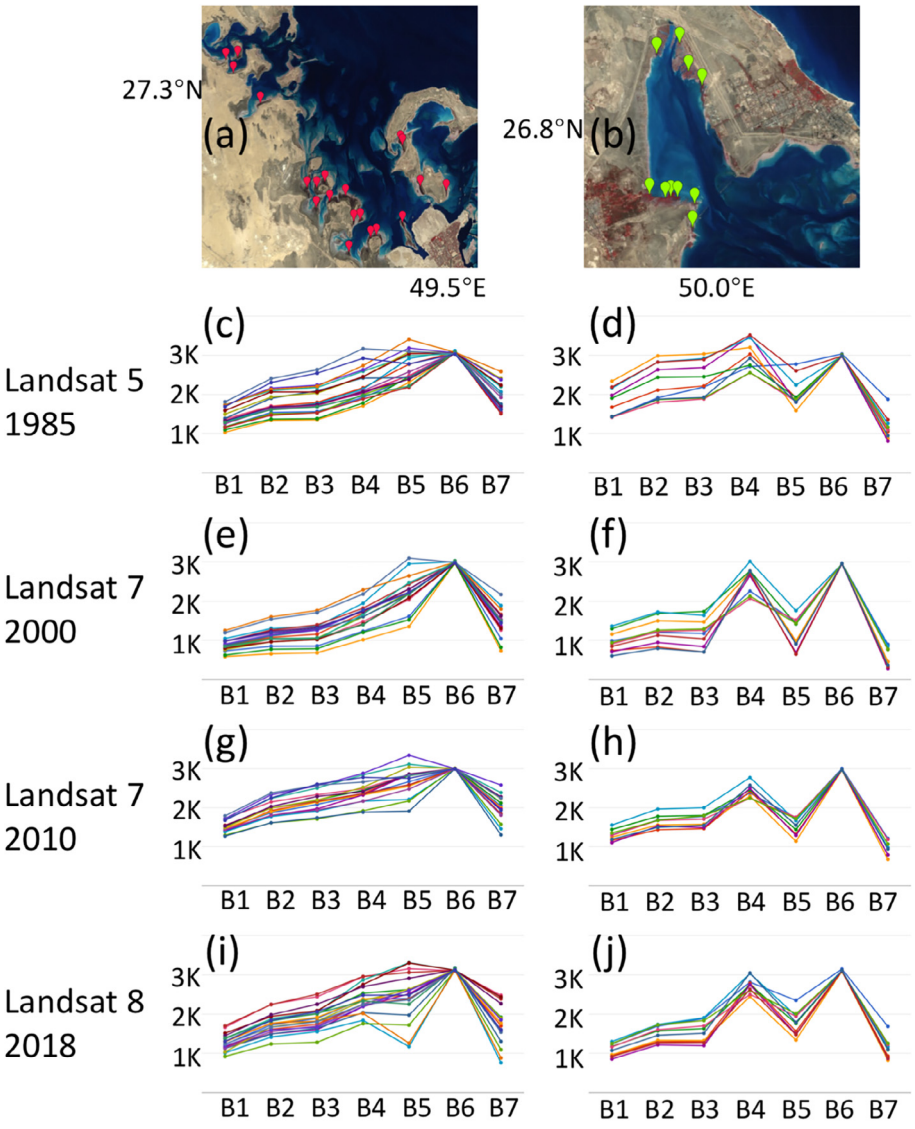

Fig. 2. Endmembers selection for spectral reflectance analysis using red and green points over (a) Jubail Conservation; (b) Tarut Bay. Red locations: classified as Mangrove forests according to USGS dataset only and Green locations: classified as Mangrove forests according to all three datasets with spectral profiles (c & d), (e & f), (g & h), (i & j) for 1985 Landsat 5, 2000 Landsat 7, 2010 Landsat 7, and 2018 Landsat 8 images, respectively.

classification models using three algorithms (CART, SVM and Random Forest) are implemented here to distinguish mangrove habitats from others.

3. Results and discussion

3.1. Comparison of existing mangrove datasets

Spectral analysis was conducted here to evaluate the data accuracy across different sources. Mangroves spectral signature is quite unique and has been correctly identified, used and compared with other sources to avoid misclassification with other marine habitats, namely salt marshes and macro algae (Benson et al., 2017; Corcoran et al., 2007; Giri, 2016; Ranjan et al., 2017). The left panel of Fig. 2 shows the spectral signature of end members from the mangrove habitat only identified by USGS Global Mangrove Forest Distribution dataset (red points in Fig. 2a). They are displayed as Landsat 5 image of 1985 in Fig. 2c, the Landsat 7 images of 2000 in Fig. 2e and 2010 in Fig. 2g, and Landsat 8 image of 2018 in Fig. 2i. The right panel of Fig. 2 shows the spectral signature of samples from mangrove habitat agreed by all of three datasets (green points in Fig. 2b). They are displayed as the Landsat 5 image of 1985 in Fig. 2d, the Landsat 7 images of 2000 in Fig. 2f and 2010 in Fig. 2h, and Landsat 8 image of 2018 in Fig. 2j. It is noteworthy that the bands in Landsat 8 are renamed to have the same spectral range of Landsat 5 and Landsat 7. It is quite evident that the spectral distributions are coherent as shown in Fig. 2(d, f, h and j), with high value at band 4 and lower value at band 5 and band 7. However, Fig. 2(c, e, g and i) does not show the same pattern – band 5 value is always higher than the value of band 4 which should not be the case. From the above and based on the conducted spectral analysis using a wide range of endmembers and comparing with established research, we believe that USGS data overestimated mangrove habitats distribution. On the other hand, the data obtained from Saudi Aramco (Loughland and Al-Abdulkader, 2011) shows the misclassified locations in the USGS dataset as saltmarsh habitats. The Landsat 5 data in 1985 was able to distinguish saltmarsh from mangroves, which is even more accurate for Landsat 7 & 8. This is because in Landsat 7 &8 the values of each band show more distinctive behavior as compared to Landsat 5 images, where all bands show less distinction Fig. 2(d, f, h and j). Considering these differences and facts between these sensors, we opted to perform the change detection analysis on the mangroves habitats using Landsat 7&8 data.

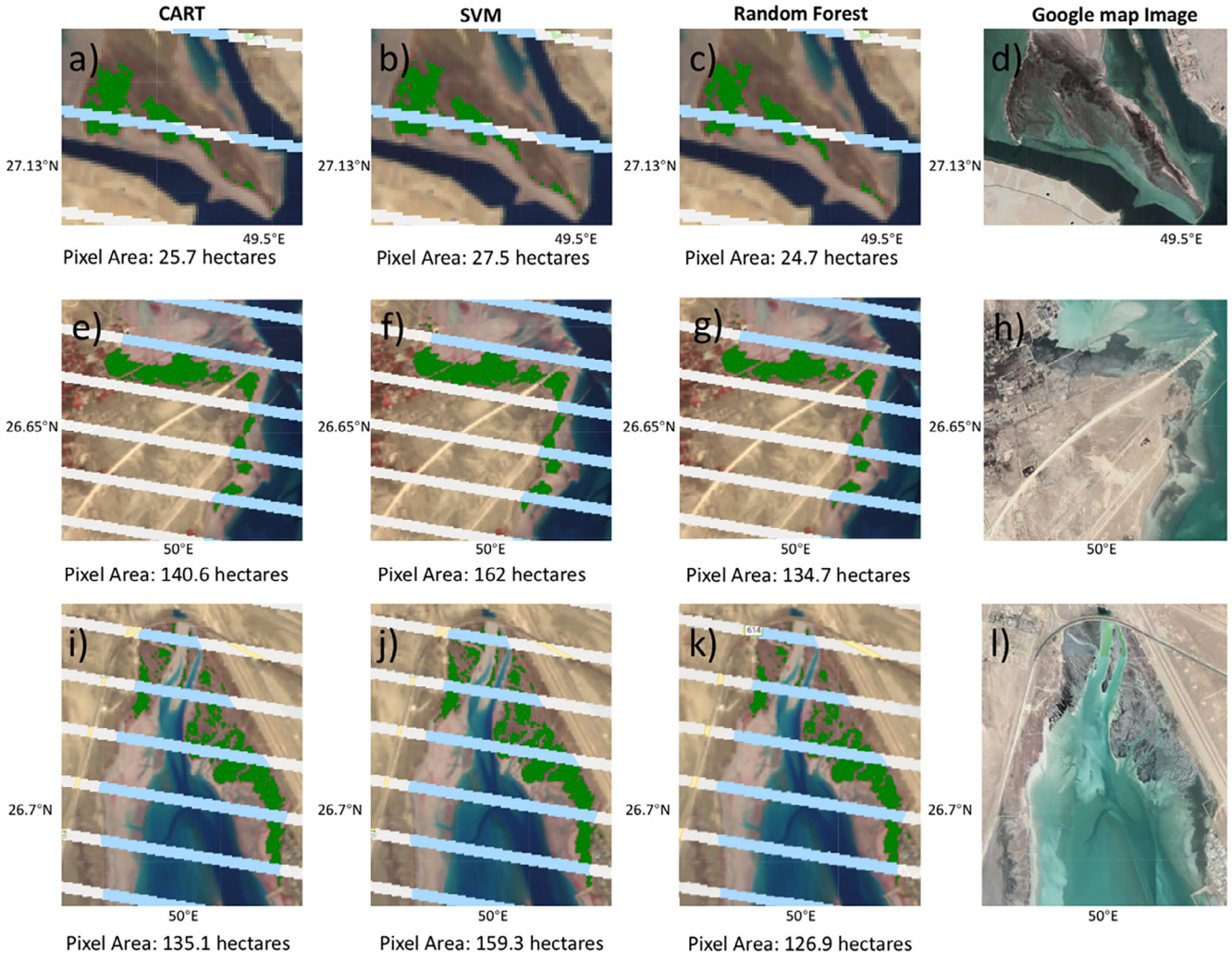

Fig. 3. Supervised classification results of Landsat 7 image of 2018 for the mangrove forests (green area) and corresponding mangrove coverage (in hectares) using CART (a, e, i), SVM (b, f, j), RF (c, g, k), compared with high resolution true colour Google Map image (d, h, l), for GI (a-d), NMTB (e-h) and NTB (i-l).

3.2. Mangrove change detection

The supervised classification models used in this study (i.e. CART, SVM and RF) were built using the same training datasets from Landsat 7 (all samples from non-gap areas) and Landsat 8 images during 2018. Five different categories, namely: arid land, mangrove, tidal flat, salt-marshes and water body were identified using 30 sample observation points per category to ensure accuracy. Training datasets accuracy was assessed against new testing datasets through computing the confusion matrix for each model. In this work we looked at the "trainAccuracy" parameter that describes how well the classifier was able to correctly label resubstituted training data (i.e. data the classifier had already seen). However, to get a true validation accuracy, we showed our three classifiers a new 'testing' data and applied the classifiers to the new testing data to assess the "errorMatrix" for this withheld validation data. The accuracy values ranged from > 95% for CART and > 90% for others, being applied on both Landsat 7 & 8.

The mangrove forests distribution following the three models are shown using Landsat 7 & 8 in the Gurmah Island (GI) (Figs. 3 and 4(a, b and c), North Middle Tarut Bay (NMTB) (Figs. 3 and 4(e, f and g)), and North Tarut Bay (NTB) (Figs. 3 and 4(i, j and k) during 2018, respectively. High resolution true color images from Google Map were included for comparison (Figs. 3 and 4 (d, h and l). The resulting pixel coverage for mangrove forests based on three classifiers, after vegetation mask (NDVI > 0.15) was applied, is computed and presented for each location. The areas of the classified mangroves (in hectares) for Landsat 7 were: SVM (GI: 27.5, NMTB: 162, NTB: 159.3) > CART (GI: 25.7, NMTB: 140.6, NTB: 135.1) > Random Forest (GI: 24.6, NMTB: 97, NTB: 111.5) and for Landsat 8 were: SVM (GI: 38.9, NMTB: 180.6, NTB: 268.7) > CART (GE: 34.8, NMTB: 151.6, NTB: 190.2) > Random Forest (GI: 31.6, NMTB: 150.5, NTB: 183.8). It is clear that SVM classifier overestimated the distribution while RF underestimated it. The three models successfully showed similar mangrove distribution over the different locations and using Landsat 7 & 8 datasets, yet we believe that CART showed the most accurate pixel coverage counting and best performance. Higher pixel coverage is expected from Landsat 8 images (Fig. 4) due to the absence of gaps exhibited in Landsat 7 data (Fig. 3). The variance in the pixel coverage following the three classifiers can be attributed to the sparse growth of mangrove habitats along coastlines, as seen from the high resolution true color composites, yet SVM failed to identify this sparsity and hence overestimated and RF did the opposite. Given the CART model higher performance and accuracy, it is now selected for the mangrove change detection analysis.

Change detection analysis is performed between 2000 and 2010 using the CART classifier based images for Landsat 7, after sub-setting our data to the previously mentioned five locations (Fig. 1) and masking terrestrial vegetation, land and water for classification purposes. Masking of terrestrial vegetation was crucial for the classification accuracy and to avoid overestimation errors by the classifiers. Landsat 7

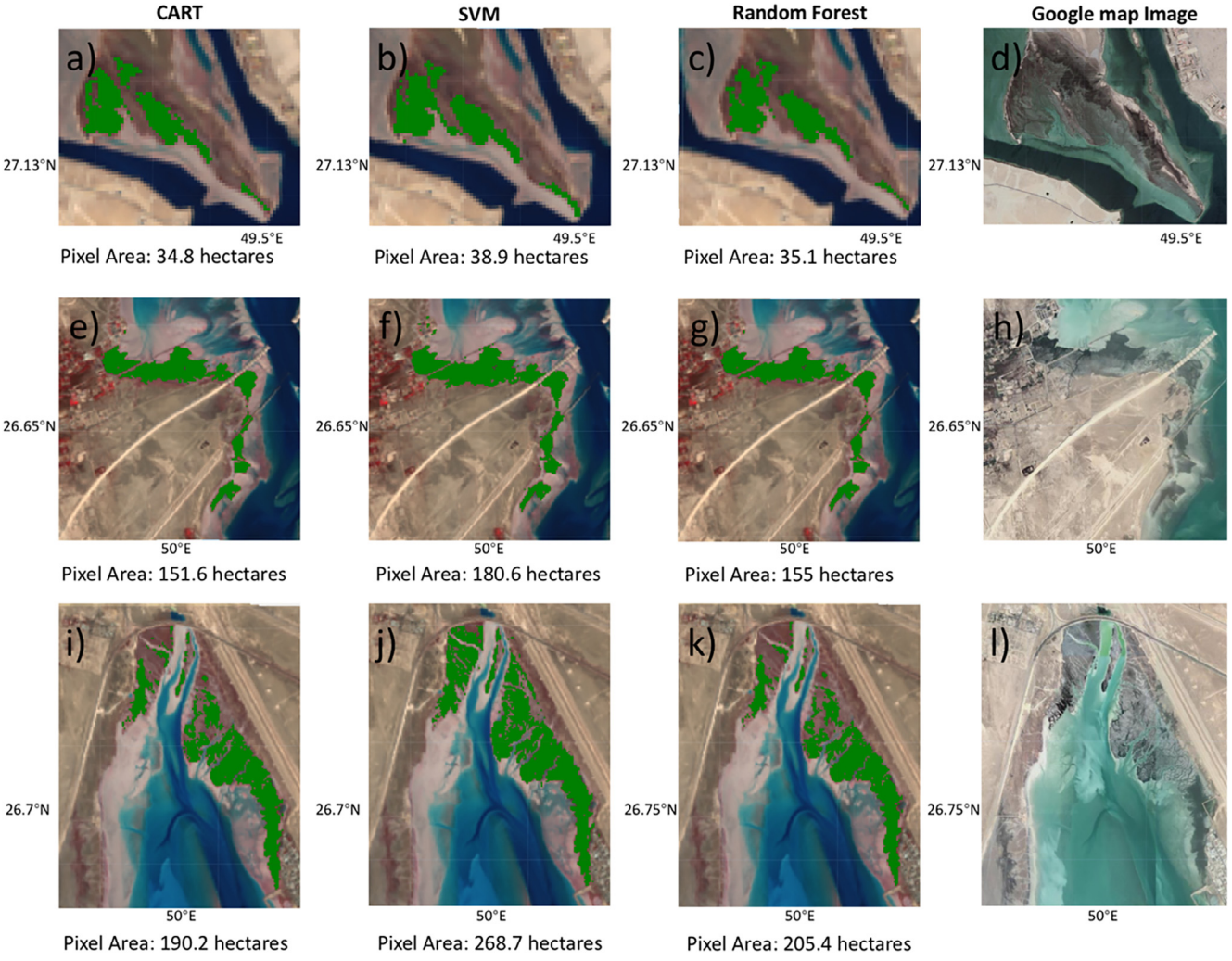

Fig. 4. Supervised classification results of Landsat 8 image of 2018 for the mangrove forests (green area) and corresponding mangrove coverage (in hectares) using CART (a, e, i), SVM (b, f, j), RF (c, g, k), compared with high resolution true colour Google Map image (d, h, l), for GI (a-d), NMTB (e-h) and NTB (i-l).

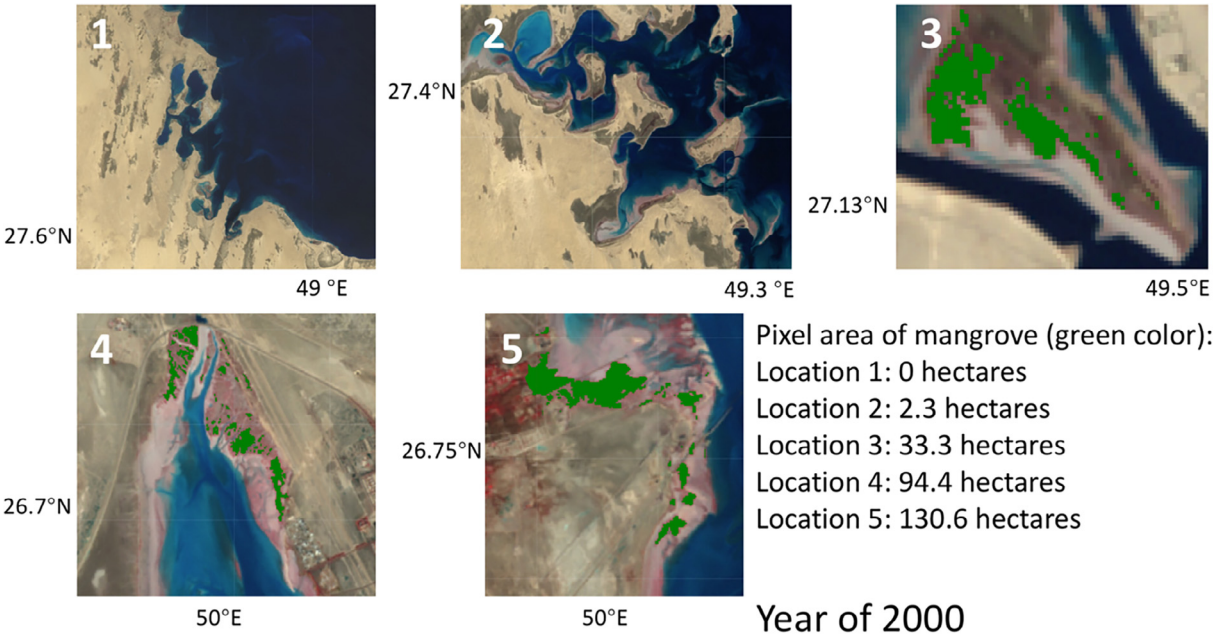

Fig. 5. Mangrove forest distribution (green area) using the CART classifier applied on Landsat 7 year 2000. The text at the right panel lists the mangrove area for each location (1–5). Refer to Fig. 1 for regions.

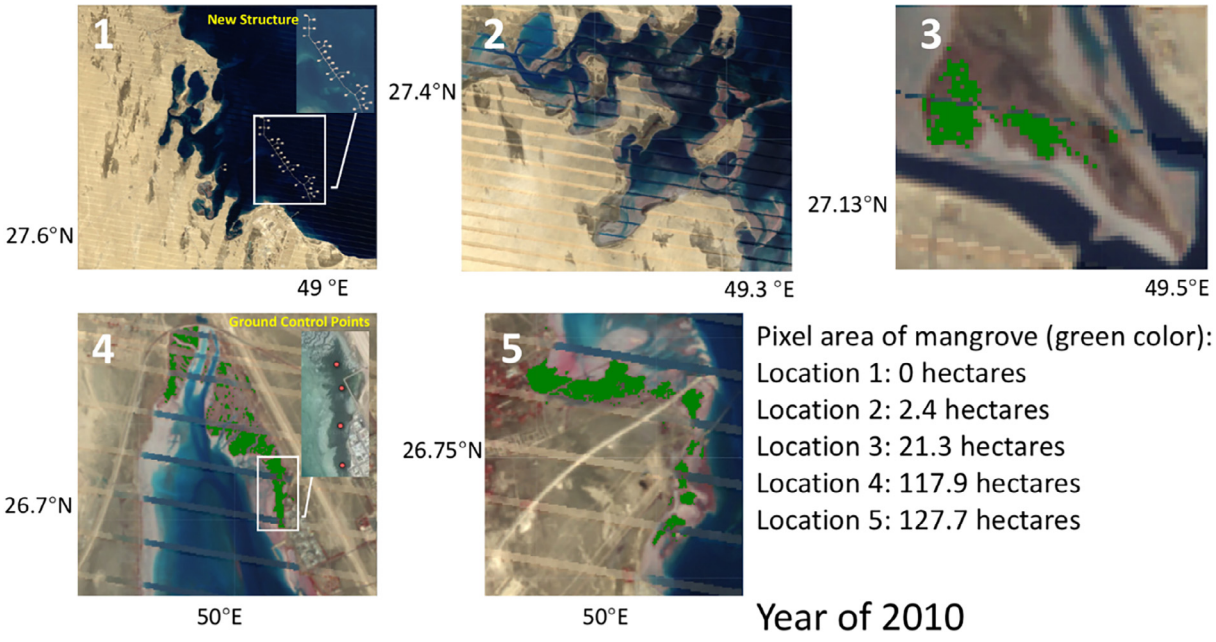

Fig. 6. Mangrove forest distribution (green area) using the CART classifier applied on Landsat 7 year 2010. The text at the right panel lists the mangrove area for each location (1–5). Refer to Fig. 1 for regions.

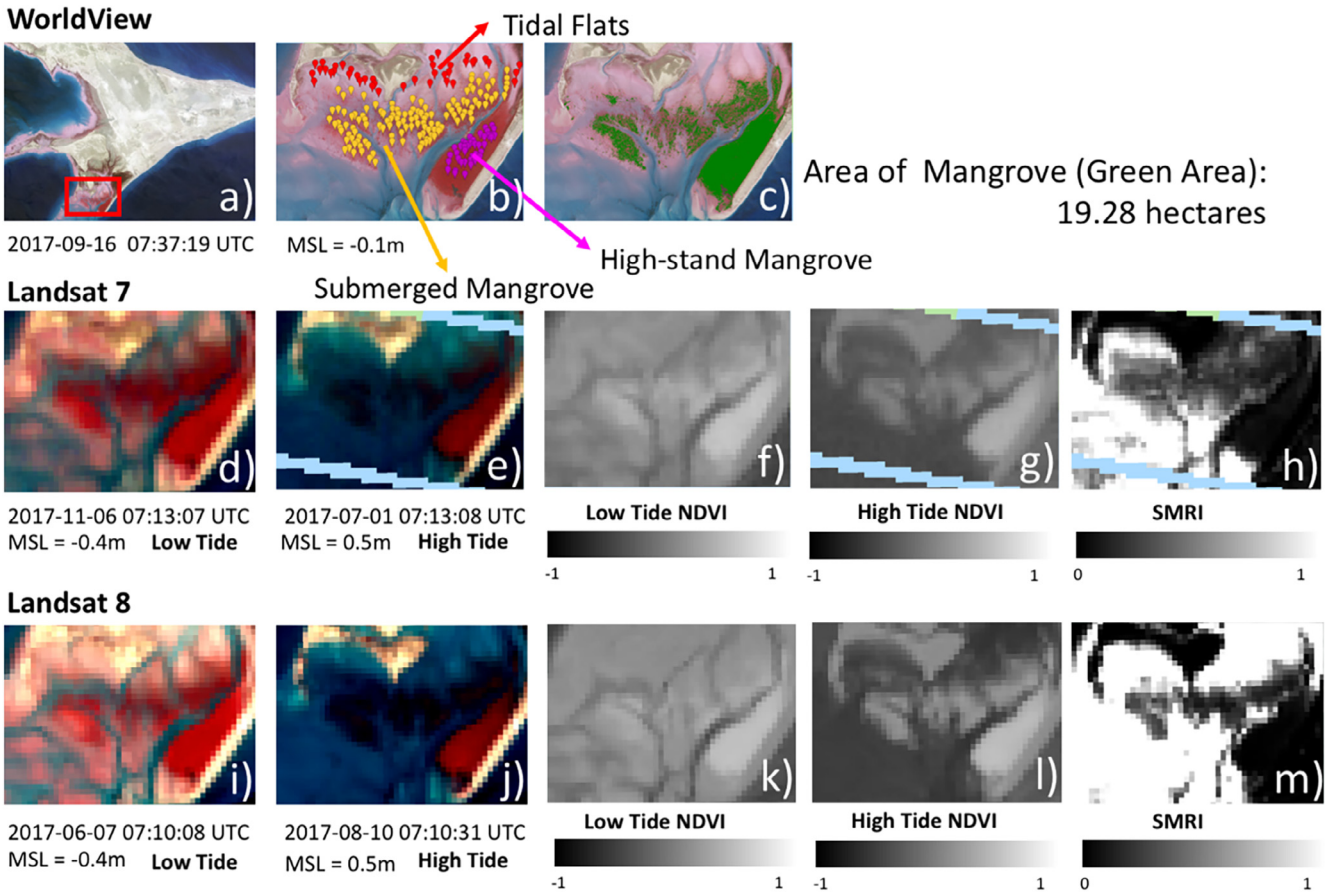

Fig. 7. WorldView-2 image of Abu Ali Island: (a) the mangrove forest in red square; (b) Sample points for tidal flats (red), high-stand mangroves (orange) and submerged mangrove (magenta); (c) Total mangrove area (green area). Landsat 7 and 8 images: (d, i) low tide; (e, j) high tide; (f, k) NDVI of low tide; (g, l) NDVI of high tide; (h, m) SMRI, respectively.

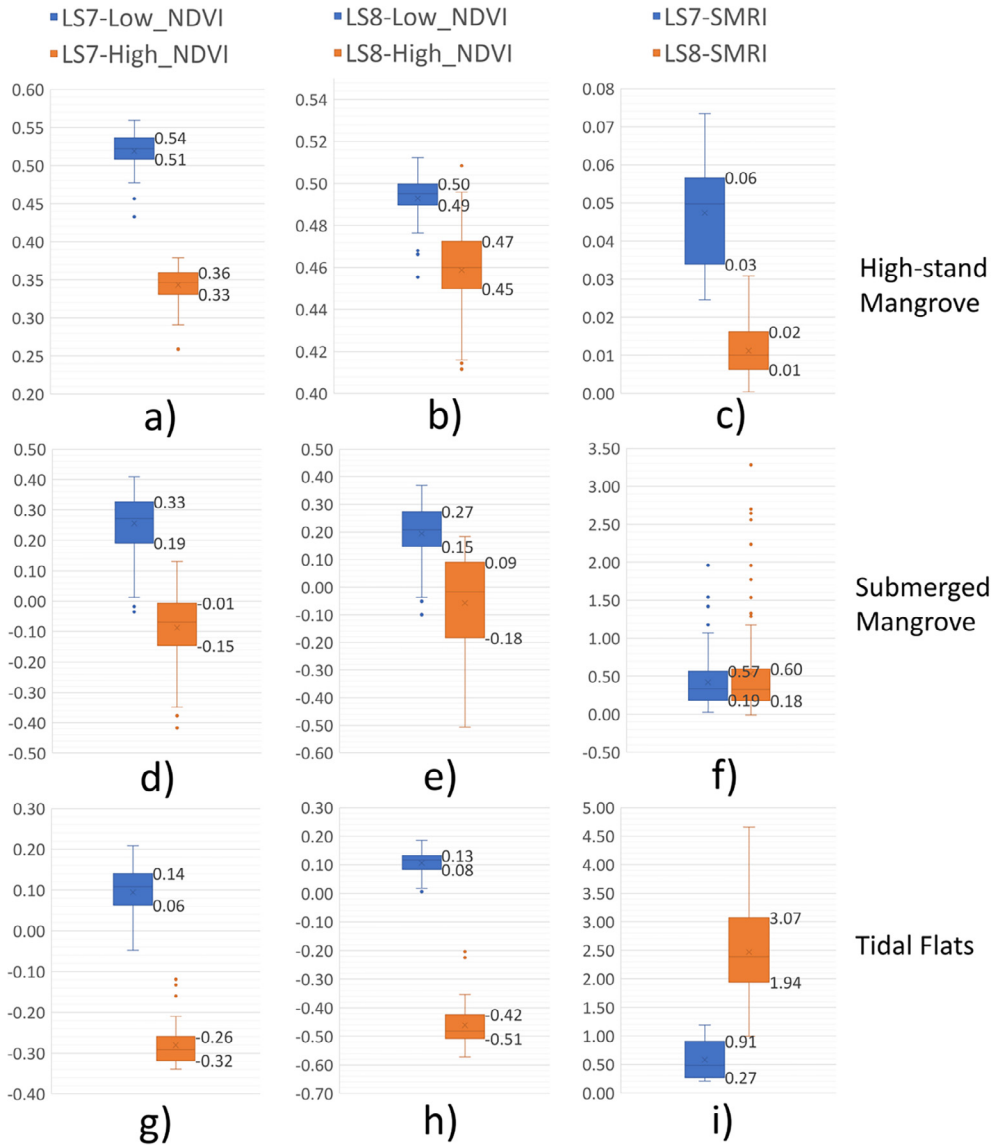

Fig. 8. First two columns: Range of NDVI values of the samples for high-stand mangrove (a,b), submerged mangrove (d,e) and tidal flats (g,h) for low tides (blue) and high tides (orange) of Landsat 7 and 8 images in Fig. 7. Third column: Range of SMRI values of the samples for high-stand mangrove (c), submerged mangrove (f) and tidal flats (i) for Landsat 7 (blue) and Landsat 8 (orange) images in Fig. 7.

is specifically selected against Landsat 8 to look at the change starting 2000 rather than 2013. Figs. 5 and 6 shows that regions 1 (Manifah) and 2 (Al-Khair) already with small mangroves fraction (0 and 2.3 ha) in 2000 exhibits almost little to no change in 2010. It is noteworthy that an artificial island was built in region 1, for ship docking and tourists (Fig. 6, region 1). Alternatively, regions 3 (GI) and 5 (NMTB), with the larger mangrove distribution (33.3 and 130.6 ha) in 2000, showed an expected decline during 2010. This may be due to coastal developments and surrounding human activities (Amin et al., 2019).

The observed increase of 0.21 km^2 over the mangrove habits in the northern Tarut Bay and Tarut Island from 2.25 km^2 to 2.46 km^2 during the period 2000–1010 matched the reported areal increase of 1.4 km^2 observed from 1999 (4 km^2) (Khan and Kumar, 2009) to 2011 (5.4 km^2) (Almahasheer et al., 2013) for the whole Tarut Bay. Moreover, the increase of 1.14 km^2 between 2010 (2.46 km^2) and 2018 (3.6 km^2) also agrees with the increasing trend of the Tarut Bay mangrove habitats from 2011 to 2014 (Al-Ali et al., 2015). However, we believe that data SLC gaps, shown as empty clear stripes, also played a role in this observation. As for region 4 (NTB) the mangrove coverage increased from (94.4 ha) in 2000 to (117.9 ha) in 2010. It is highly likely that these classification results using gap-filled image by GEE mosaicking method contributed to this increase in the mangroves distribution that was validated with ground observations over some of the gap areas (Fig. 6, region 4). It is clear that mangrove biomass and distribution in NTB has unexpectedly increased from 94.4 to 117.9 to 190.2 ha during 2000 (Fig. 5 region 4), 2010 (Fig. 6 region 4) and 2018 (Fig. 4i). Data filling may have contributed to better accuracy; however, tide levels also affect mangroves that is evident from their divergent spectral properties in high/low water levels. This will be discussed further in the next section.

3.3. Submerged mangrove detection

As mentioned above, tidal levels could have an impact on mangrove mapping and detection. SMRI was generated from low and high tides on the Abu Ali Island located in region 3 (Jubail), to use the unique spectral signature of submerged mangroves forest to distinguish them by different tide levels. The WorldView-2 high resolution images of Abu Ali Island show mangrove forests in the south coast highlighted by the red square (Fig. 7a). Fig. 7b shows the sample points for dense high-

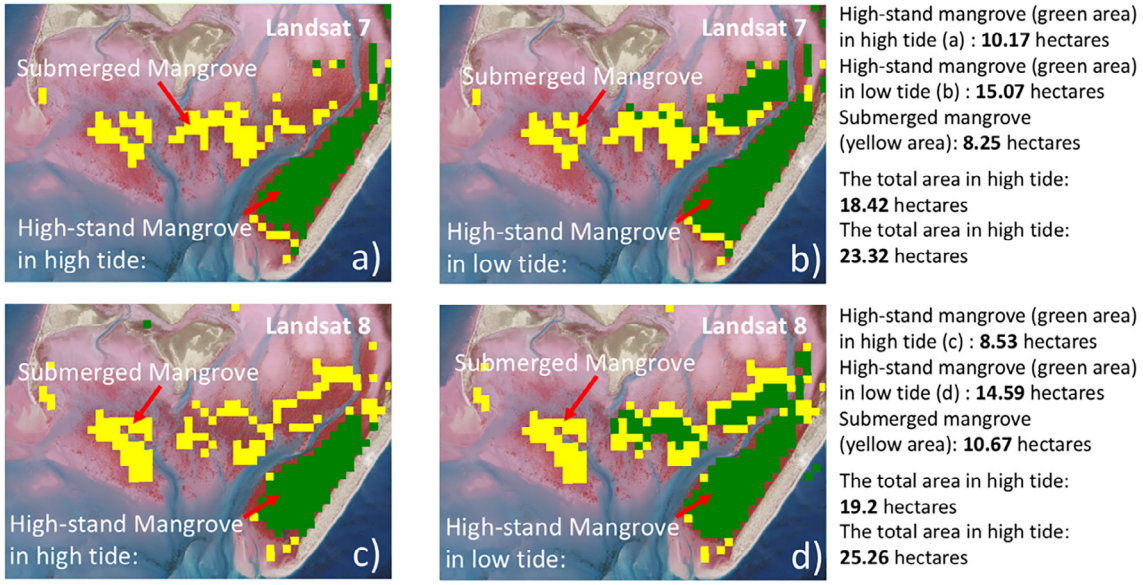

Fig. 9. (a) High-stand mangrove forests (green area) in high tide of Fig. 7e; SMRI indicated submerged mangrove forests (yellow area). (b) High-stand mangrove forests (green area) in low tide of Fig. 7d; same submerged mangrove forests as Fig. 9a. (d) High-stand mangrove forests (green area) and in high tide of Fig. 7j; SMRI indicated submerged mangrove forests (yellow area). (b) High-stand mangrove forests (green area) in low tide of Fig. 7i; same submerged mangrove forests as Fig. 9c. The text at the very right panel lists the mangrove area.

stand mangroves in the south east corner (magenta points), tidal submerged mangrove in the middle (orange points), and tidal flats (red points). The mangroves total area, including tidal and non-tidal areas, was calculated using the K-means classification method applied on Fig. 7b and was found to be 19.28 ha (see green area in Fig. 7c). To assess tidal impacts on mangrove distribution, the mean sea level (MSL) data was also used, mentioned above in the data section. False color composites for the region at low tides (MSL = -0.4 m) and high tides (MSL = 0.5) are shown in Fig. 7(d & e) for Landsat 7 and Fig. 7(i & j) for Landsat 8, respectively. It is noteworthy that Landsat 7 SLC failure gaps did not intercede the areas of mangrove forests in the case of Abu Ali Island. Fig. 7(d & i) representing mangroves at low tides (marked as the red vegetation) from Landsat 7 & 8 exhibits larger distribution than the submerged mangroves that almost disappeared during the high tides (Fig. 7(e & j). This indicates that change detection analysis of such area could be dramatically altered if images are not compared at the same water level. The NDVI images of low tides (Fig. 7f & k), and high tides (Fig. 7g & l) show that the NDVI index could be helpful to distinguish high-stand mangrove from others, but fails to discriminate the submerged mangroves and tidal flats in low tides, as well as submerged mangrove and land. While in the SMRI images (Fig. 7h & m), submerged mangroves could be seen as grey areas. The SMRI images indicate that: 1) for non-tidal regions such as land or high-stand mangrove, the SMRI value is close to 0; 2) for non-vegetation tidal flats regions, the SMRI value could be very high above 1 (Fig. 7m), but also could be closer to submerged mangrove. One can use the spectral properties of submerged mangrove and tidal flats under high tides condition to separate them.

Fig. 8 exhibits the ranges of NDVI and SMRI values of the samples for high-stand mangrove (Fig. 8a-c), submerged mangrove (Fig. 8d-e) and tidal flats (Fig. 8g-i) in Landsat 7&8 images displayed in Fig. 7. The NDVI values in low tides are higher than those in high tides in general. However, NDVI values of Landsat 8 images between tide levels are very close as seen in Fig. 8b. In the Fig. 8f, the SMRI values have very similar ranges (0.18 to 0.60 and 0.19 to 0.57) regardless of the different satellite images. This proves the robustness of SMRI as a submerged mangrove detection method. However, the ranges of SMRI values for Landsat 7 are overlapped between submerged mangroves and tidal flats (Fig. 8f and 8i). This could be solved by applying the divergence of high tide NDVI values for submerged mangrove (-0.18 to 0.09 in Fig. 8e) and tidal flats (-0.51 to -0.42) in Fig. 8h), which could be used to mask out tidal flats from SMRI-indicated mangrove areas.

Fig. 9 shows the detection results for both high-stand mangrove as green areas using K-means unsupervised method, and submerged mangrove as yellow areas by choosing regions with SMRI values (0.18–0.60 for Landsat 7, 0.19–0.57 for Landsat 8, then masking with high tide NDVI > -0.2). The areas of submerged mangroves are 8.25 and 10.67 ha for Landsat 7 and Landsat 8 images, respectively. The classified mangrove areas of Fig. 9(b & d) cover most of the targeted mangrove areas shown in the background using the high resolution WorldView-2 image. The summation of high-stand mangrove in high tide and submerged mangrove areas (19.2 ha using Landsat 8, 18.42 ha using Landsat 7) are very close to high resolution WorldView-2 image result (19.28 ha), indicating that this approach could provide an effective estimate and addresses the tidal impact on mangrove mapping.

4. Conclusions

The spatial distribution and spatial-temporal changes of mangrove forests in Arabian Gulf along the Saudi Arabia during the period of 2000 to 2018 were explored using large data sets and spatial analysis. First, we compared the spectral reflectance signatures between identified mangrove forest and other coastal vegetation habitats (such as seagrasses and saltmarshes) using Landsat 5&7&8 data. Mangrove habitat detection in the WAG was carried out through the evaluation of the three widely-used mangrove classification methods, namely Supported Vector Machine (SVM), Classification and Regression Trees (CART) and Random Forest (RF). CART was validated as the most effective classifier (accuracy > 95%) for WAG mangrove detestation. Later, we used the medium-resolution Landsat 7&8 images to build a CART-based mangrove supervised classification model to obtain mangrove areas and distributions for 2000, 2010 and 2018. With both Landsat and the high resolution WorldView-2 images, the new SMRI method was applied in the area of Abu Ali Islands with the usage of K-means unsupervised method to identify and evaluate the biomass and distribution of submerged mangroves in the tidal area. We investigated the protocol to detect overall mangrove distribution from samples taken from Abu Ali Island with indices SMRI and NDVI values generated from

Landsat 7&8 images. By employing these two indices, there was a good match between the estimates of the mangrove area to the south of Abu Ali Island at 19.20 ha using Landsat 8 and 19.28 ha calculated from the high resolution WorldView-2. This studies presents a unique approach of SMRI to detect mangroves with historical Landsat images that has historical record and can be used to address tidal impacts on mangrove mapping and areas estimation over different locations, which could achieve more accurate outcomes of mangrove detection within limited usage of costly high resolution remote sensing imagery.

Acknowledgements

The authors would like to acknowledge the use of the Samueli Laboratory in Computational Sciences in the Schmid College of Science and Technology, Chapman University for data processing and analysis. We would also like to acknowledge the Center for Environment and Water, King Fahd University of Petroleum and Minerals (KFUPM), Saudi Arabia for conducting field measurements for use in further comparisons and validations studies. Jingjing Li would also like to acknowledge the support through the NASA Minority University Research and Education Project (MUREP) Institutional Research Opportunity grant number [NNX15AQ06A].

References

Ahamed, T., Tian, L., Zhang, Y., Ting, K.C., 2011. A review of remote sensing methods for biomass feedstock production. Biomass Bioenergy 35, 2455–2469. https://doi.org/10.1016/j.biombioe.2011.02.028.

Al-Ali, A.M., Del Campo, A.G., Rocha, C., 2015. Environmental assessment of mangrove communities in Tarut bay, eastern Arabian Peninsula, based on multidisciplinary approach. In: International Archives of the Photogrammetry, Remote Sensing and Spatial Information Sciences—ISPRS Archives, (7W3 ed., Vol. 40, pp. 269–276). doi: 10.5194/isprsarchives-XL-7-W3-269-2015.

Al-Kahtany, K., El-Sorogy, A., Al-Kahtany, F., Youssef, M., 2018. Heavy metals in mangrove sediments of the central Arabian Gulf shoreline, Saudi Arabia. Arabian J. Geosci. 11. https://doi.org/10.1007/s12517-018-3463-0.

Almahasheer, H., 2018. Spatial coverage of mangrove communities in the Arabian Gulf. Environ. Monit. Assess. 190. https://doi.org/10.1007/s10661-018-6472-2.

Almahasheer, H., 2019. High levels of heavy metals in Western Arabian Gulf mangrove soils. Mol. Biol. Rep. https://doi.org/10.1007/s11033-019-04603-2.

Almahasheer, H., Al-Taisan, W., Mohamed, M.K., 2013. Mangrove deterioration in Tarut Bay on the Eastern Province of the Kingdom of Saudi Arabia. Pakhtunkhwa J. Life Sci. 01, 49–59.

Al-Maslamani, I., Walton, M.E.M., Kennedy, H.A., Al-Mohannadi, M., Le Vay, L., 2013. Are mangroves in arid environments isolated systems? Life-history and evidence of dietary contribution from inwelling in a mangrove-resident shrimp species. Estuar. Coast. Shelf Sci. 124, 56–63. https://doi.org/10.1016/j.ecss.2013.03.007.

Al-Muzaini, S., Jacob, P.G., 1996. Marine plants of the Arabian Gulf. Environ. Int. 22, 369–376. https://doi.org/10.1016/0160-4120(96)00023-2.

Alongi, D.M., 2002. Present state and future of the world's mangrove forests. Environ. Conserv. 29. https://doi.org/10.1017/S0376892902000231.

Amahasheer, H., Aljowair, A., Duarte, C.M., Irigoien, X., 2016. Decadal stability of Red Sea mangroves. Estuar. Coast. Shelf Sci. 169, 164–172. https://doi.org/10.1016/j.ecss.2015.11.027.

Amin, S., Fouad, M., Ataisan, W., Zyadah, M., n.d. Human, Urban and Environmental-Induced Alterations in Mangroves Pattern along Arabian Gulf Coast, Eastern Province, KSA. doi: 10.20944/preprints201801.0259.v1.

Assessment, M.E. Millennium Ecosystem Assessment Findings; Millennium Ecosystem Assessment: Washington, DC, USA, 2005. 9.

Benson, L., Glass, L., Jones, T., Ravaoarinorotsihoarana, L., Rakotomahazo, C., 2017. Mangrove carbon stocks and ecosystem cover dynamics in southwest Madagascar and the implications for local management. Forests 8, 190. https://doi.org/10.3390/f8060190.

Bird, E., 2010. Saudi Arabia, Persian Gulf Coast. In: Bird, E.C.F. (Ed.), Encyclopedia of the World's Coastal Landforms. Springer Netherlands, Dordrecht, pp. 1045–1046. https://doi.org/10.1007/978-1-4020-8639-7_194.

Breiman, L. (Ed.), 1998. Classification and regression trees, Repr. ed. Chapman & Hall [u. a.], Boca Raton.

Burt, J.A., 2014. The environmental costs of coastal urbanization in the Arabian Gulf. City 18, 760–770. https://doi.org/10.1080/13604813.2014.962889.

Collins, D.S., Avdis, A., Allison, P.A., Johnson, H.D., Hill, J., Piggott, M.D., Hassan, M.H.A., Damit, A.R., 2017. Tidal dynamics and mangrove carbon sequestration during the Oligo-Miocene in the South China Sea. Nat. Commun. 8, 15698. https://doi.org/10.1038/ncomms15698.

Corcoran, E., Ravilious, C., Skuja, M., 2007. Mangroves of Western and Central Africa. UNEP-WCMC Biodiversity Series (UNEP).

Danielsen, F., 2005. The Asian Tsunami: a protective role for coastal vegetation. 643–643. Science 310. https://doi.org/10.1126/science.1118387.

Dinesh, R., Ghoshal Chaudhuri, S., 2013. Soil biochemical/microbial indices as ecological indicators of land use change in mangrove forests. Ecol. Ind. 32, 253–258. https://doi.org/10.1016/j.ecolind.2013.03.035.

Donato, D.C., Kauffman, J.B., Murdiyarso, D., Kurnianto, S., Stidham, M., Kanninen, M., 2011. Mangroves among the most carbon-rich forests in the tropics. Nat. Geosci. 4, 293–297. https://doi.org/10.1038/ngeo1123.

Duke, N.C., Meynecke, J.-O., Dittmann, S., Ellison, A.M., Anger, K., Berger, U., Cannicci, S., Diele, K., Ewel, K.C., Field, C.D., Koedam, N., Lee, S.Y., Marchand, C., Nordhaus, I., Dahdouh-Guebas, F., 2007. A world without mangroves? Science 317, 41b–42b. https://doi.org/10.1126/science.317.5834.41b.

Duro, D.C., Franklin, S.E., Dubé, M.G., 2012. A comparison of pixel-based and object-based image analysis with selected machine learning algorithms for the classification of agricultural landscapes using SPOT-5 HRG imagery. Remote Sens. Environ. 118, 259–272. https://doi.org/10.1016/j.rse.2011.11.020.

El-Askary, H., El-Mawla, S.H.A., Li, J., El-Hattab, M.M., El-Raey, M., 2014. Change detection of coral reef habitat using Landsat-5 TM, Landsat 7 ETM+ and Landsat 8 OLI data in the Red Sea (Hurghada, Egypt). Int. J. Remote Sens. 35, 2327–2346. https://doi.org/10.1080/01431161.2014.894656.

Ellis, W.L., Bell, S.S., 2013. Intertidal fish communities may make poor indicators of environmental quality: lessons from a study of mangrove habitat modification. Ecol. Indic. 24, 421–430. https://doi.org/10.1016/j.ecolind.2012.07.008.

Faridah-Hanum, I., Yusoff, F.M., Fitrianto, A., Ainuddin, N.A., Gandaseca, S., Zaiton, S., Norizah, K., Nurhidayu, S., Roslan, M.K., Hakeem, K.R., Shamsuddin, I., Adnan, I., Awang Noor, A.G., Balqis, A.R.S., Rhyma, P.P., Siti Aminah, I., Hilaluddin, F., Fatin, R., Harun, N.Z.N., 2019. Development of a comprehensive mangrove quality index (MQI) in Matang Mangrove: assessing mangrove ecosystem health. Ecol. Ind. 102, 103–117. https://doi.org/10.1016/j.ecolind.2019.02.030.

Foody, G.M., Mathur, A., 2006. The use of small training sets containing mixed pixels for accurate hard image classification: training on mixed spectral responses for classification by a SVM. Remote Sens. Environ. 103, 179–189. https://doi.org/10.1016/j.rse.2006.04.001.

Giri, C., 2016. Observation and monitoring of mangrove forests using remote sensing: opportunities and challenges. Remote Sens. 8, 783. https://doi.org/10.3390/rs8090783.

Giri, C., Ochieng, E., Tieszen, L.L., Zhu, Z., Singh, A., Loveland, T., Masek, J., Duke, N., 2011. Status and distribution of mangrove forests of the world using earth observation satellite data: status and distributions of global mangroves. Glob. Ecol. Biogeogr. 20, 154–159. https://doi.org/10.1111/j.1466-8238.2010.00584.x.

Giri, C., Long, J., Abbas, S., Murali, R.M., Qamer, F.M., Pengra, B., Thau, D., 2015. Distribution and dynamics of mangrove forests of South Asia. J. Environ. Manage. 148, 101–111. https://doi.org/10.1016/j.jenvman.2014.01.020.

Gitelson, A.A., Kaufman, Y.J., Merzlyak, M.N., 1996. Use of a green channel in remote sensing of global vegetation from EOS-MODIS. Remote Sens. Environ. 58, 289–298. https://doi.org/10.1016/S0034-4257(96)00072-7.

Green, E.P., Mumby, P.J., Edwards, A.J., Clark, C.D., Ellis, A.C., 1998. The assessment of mangrove areas using high resolution multispectral airborne imagery. J. Coastal Res. 433–443.

Heenkenda, M., Joyce, K., Maier, S., Bartolo, R., 2014. Mangrove species identification: comparing WorldView-2 with aerial photographs. Remote Sens. 6, 6064–6088. https://doi.org/10.3390/rs6076064.

Heenkenda, M.K., Joyce, K.E., Maier, S.W., de Bruin, S., 2015. Quantifying mangrove chlorophyll from high spatial resolution imagery. ISPRS J. Photogramm. Remote Sens. 108, 234–244. https://doi.org/10.1016/j.isprsjprs.2015.08.003.

Heumann, B.W., 2011. An object-based classification of mangroves using a hybrid decision tree—support vector machine approach. Remote Sens. 3, 2440–2460. https://doi.org/10.3390/rs3112440.

Hutchison, J., Manica, A., Swetnam, R., Balmford, A., Spalding, M., 2014. Predicting global patterns in mangrove forest biomass: global patterns in mangrove biomass. Conserv. Lett. 7, 233–240. https://doi.org/10.1111/conl.12060.

Kanniah, K., Sheikhi, A., Cracknell, A., Goh, H., Tan, K., Ho, C., Rasli, F., 2015. Satellite images for monitoring mangrove cover changes in a fast growing economic region in Southern Peninsular Malaysia. Remote Sensing 7, 14360–14385. https://doi.org/10.3390/rs71114360.

Kathiresan, K., Rajendran, N., 2005. Coastal mangrove forests mitigated tsunami. Estuar. Coast. Shelf Sci. 65, 601–606. https://doi.org/10.1016/j.ecss.2005.06.022.

Khan, M.A., Kumar, A., 2009. Impact of "urban development" on mangrove forests along the west coast of the Arabian Gulf. E-journal Earth Sci. India 2, 159–173.

Kim, S.-R., Prasad, A.K., El-Askary, H., Lee, W.-K., Kwak, D.-A., Lee, S.-H., Kafatos, M., 2014. Application of the Savitzky-Golay filter to land cover classification using temporal MODIS vegetation indices. Photogramm. Eng. Remote Sens. 80, 675–685. https://doi.org/10.14358/PERS.80.7.675.

Lawrence, R.L., Andrea, W., 2001. Rule-based classification systems using classification and regression tree (CART) analysis. Photogramm. Eng. Remote Sens. 67 (10), 1137–1142.

Le Louarn, M., Clergeau, P., Briche, E., Deschamps-Cottin, M., 2017. "Kill two birds with one stone": urban tree species classification using bi-temporal Pléiades images to study nesting preferences of an invasive bird. Remote Sens. 9, 916. https://doi.org/10.3390/rs9090916.

Li, W., El-Askary, H., ManiKandan, K., Qurban, M., Garay, M., Kalashnikova, O., 2017. Synergistic use of remote sensing and modeling to assess an anomalously high chlorophyll-a event during summer 2015 in the South Central Red Sea. Remote Sens. 9, 778. https://doi.org/10.3390/rs9080778.

Li, W., El-Askary, H., Qurban, M., Proestakis, E., Garay, M., Kalashnikova, O., Amiridis, V., Gkikas, A., Marinou, E., Piechota, T., Manikandan, K., 2018. An assessment of atmospheric and meteorological factors regulating red sea phytoplankton growth. Remote Sens. 10, 673. https://doi.org/10.3390/rs10050673.

Li, M., Ma, L., Blaschke, T., Cheng, L., Tiede, D., 2016. A systematic comparison of different object-based classification techniques using high spatial resolution imagery in agricultural environments. Int. J. Appl. Earth Observ. Geoinf. 49, 87–98. https://doi.org/10.1016/j.jag.2016.01.011.

Li, M.S., Mao, L.J., Shen, W.J., Liu, S.Q., Wei, A.S., 2013. Change and fragmentation trends of Zhanjiang mangrove forests in southern China using multi-temporal Landsat imagery (1977–2010). Estuar. Coast. Shelf Sci. 130, 111–120. https://doi.org/10.1016/j.ecss.2013.03.023.

Loughland, R.A., Al-Abdulkader, K.A., 2011. Marine atlas, Western Arabian Gulf. Saudi Aramco, Environment Protection Dept.: Center for Environment & Water Research Institute, KFUPM, Dhahran, Saudi Arabia.

Moore, G.E., Grizzle, R.E., Ward, K.M., Alshihi, R.M., 2015. Distribution, pore-water chemistry, and stand characteristics of the mangroves of the United Arab Emirates. J. Coastal Res. 314, 957–963. https://doi.org/10.2112/JCOASTRES-D-14-00142.1.

Mutanga, O., Adam, E., Cho, M.A., 2012. High density biomass estimation for wetland vegetation using worldview-2 imagery and random forest regression algorithm. Int. J. Appl. Earth Obs. Geoinform. 18, 399–406.

Naser, H., Hoad, G., 2011. An investigation of salinity tolerance and salt secretion in protected mangroves, Bahrain. Gulf II: an international conference. The state of the Gulf ecosystem: Functioning and services. Kuwait City, Kuwait. 7-9 February 2011.

Ng, W.-T., Rima, P., Einzmann, K., Immitzer, M., Atzberger, C., Eckert, S., 2017. Assessing the potential of Sentinel-2 and Pléiades data for the detection of Prosopis and Vachellia spp. in Kenya. Remote Sens. 9, 74. https://doi.org/10.3390/rs9010074.

Pal, M., Mather, P.M., 2005. Support vector machines for classification in remote sensing. Int. J. Remote Sens. 26, 1007–1011. https://doi.org/10.1080/01431160512331314083.

Pantaleoni, E., Wynne, R.H., Galbraith, J.M., Campbell, J.B., 2009. Mapping wetlands using ASTER data: a comparison between classification trees and logistic regression. Int. J. Remote Sens. 30, 3423–3440. https://doi.org/10.1080/01431160802562214.

Pimple, U., Simonetti, D., Sitthi, A., Pungkul, S., Leadprathom, K., Skupek, H., Som-ard, J., Gond, V., Towprayoon, S., 2018. Google earth engine based three decadal landsat imagery analysis for mapping of mangrove forests and its surroundings in the Trat Province of Thailand. J. Comput. Commun. 06, 247–264. https://doi.org/10.4236/jcc.2018.61025.

Price, A.R.G., Sheppard, C.R.C., Roberts, C.M., 1993. The Gulf: its biological setting. Mar. Pollut. Bull. 27, 9–15. https://doi.org/10.1016/0025-326X(93)90004-4.

Ranjan, A.K., Sivathanu, V., Verma, S.K., Murmu, L., Kumar, P.B.S., 2017. Spatio-temporal variation in Indian part of Sundarban Delta over the years 1990–2016 using Geospatial Technology. Int. J. Geomatics Geosci. 7, 275–292.

Rogers, K., Lymburner, L., Salum, R., Brooke, B.P., Woodroffe, C.D., 2017. Mapping of mangrove extent and zonation using high and low tide composites of Landsat data. Hydrobiologia 803, 49–68. https://doi.org/10.1007/s10750-017-3257-5.

Rouse, J., Haas, R., Schell, J., Deering, D., editors, 1973. Monitoring vegetation systems in the Great Plains with ERTS. Third ERTS symposium: NASA SP-351. pp. 309–317.

Saudi-Aramco, 2016. Saudi Aramco Biodiversity Protection Areas. IPIECA, http://www.ipieca.org/media/2781/saudi_aramco_biodiversity_protection_areas.pdf.

Shapiro, A., Trettin, C., Küchly, H., Alavinapanah, S., Bandeira, S., 2015. The mangroves of the Zambezi Delta: increase in extent observed via satellite from 1994 to 2013. Remote Sens. 7, 16504–16518. https://doi.org/10.3390/rs71215838.

Spalding, M., Kainuma, M., Collins, L., 2010. World atlas of mangroves.

Su, Y., Ma, Q., Guo, Q., 2017. Fine-resolution forest tree height estimation across the Sierra Nevada through the integration of spaceborne LiDAR, airborne LiDAR, and optical imagery. Int. J. Digital Earth 10, 307–323. https://doi.org/10.1080/17538947.2016.1227380.

Vincini, M., Frazzi, E., D'Alessio, P., 2007. Comparison of narrow-band and broad-band vegetation indexes for canopy chlorophyll density estimation in sugar beet. In: Proceedings of the 6th European Conference on Precision Agriculture '07. Wageningen, The Netherlands. pp. 189–196.

Vincini, M., Frazzi, E., D'Alessio, P., 2008. A broad-band leaf chlorophyll vegetation index at the canopy scale. Precis. Agric. 9, 303–319. https://doi.org/10.1007/s11119-008-9075-z.

Vo, Q.T., Kuenzer, C., Vo, Q.M., Moder, F., Oppelt, N., 2012. Review of valuation methods for mangrove ecosystem services. Ecol. Ind. 23, 431–446. https://doi.org/10.1016/j.ecolind.2012.04.022.

Wang, D., Wan, B., Qiu, P., Su, Y., Guo, Q., Wu, X., 2018. Artificial mangrove species mapping using Pléiades-1: an evaluation of pixel-based and object-based classifications with selected machine learning algorithms. Remote Sens. 10, 294. https://doi.org/10.3390/rs10020294.

Whitney, K., Scudiero, E., El-Askary, H.M., Skaggs, T.H., Allali, M., Corwin, D.L., 2018. Validating the use of MODIS time series for salinity assessment over agricultural soils in California, USA. Ecol. Ind. 93, 889–898. https://doi.org/10.1016/j.ecolind.2018.05.069.

Xia, Q., Qin, C.-Z., Li, H., Huang, C., Su, F.-Z., 2018. Mapping mangrove forests based on multi-tidal high-resolution satellite imagery. Remote Sens. 10, 1343. https://doi.org/10.3390/rs10091343.

Zhao, S., Liu, Y., Jiang, J., Cheng, W., Zhou, M., Li, M., Ruan, R., 2014. Extraction of mangrove in Hainan Dongzhai Harbor based on CART decision tree. In: 2014 22nd International Conference on Geoinformatics. Presented at the 2014 22nd International Conference on Geoinformatics. IEEE, Kaohsiung, Taiwan, pp. 1–6. https://doi.org/10.1109/GEOINFORMATICS.2014.6950800.